Machine Learning Empowered Thin Film Acoustic Wave Sensing

Kaitao Tan[#,1], Zhangbin Ji[#,1], Jian Zhou[*,1], Zijing Deng[1], Songsong Zhang[2], Yuandong Gu[2], Yihao Guo[1], Fengling Zhuo[1], Huigao Duan[1], YongQing Fu[3]

1 College of Mechanical and Vehicle Engineering, Hunan University, Changsha 410082, China
2 Shanghai Industrial μTechnology Research Institute (SITRI), 235 Chengbei Rd, 201800 Shanghai, China
3 Faculty of Engineering and Environment, Northumbria University, Newcastle upon Tyne NE1 8ST, United Kingdom

The same contributions

* Corresponding E-mail: jianzhou@hnu.edu.cn

ABSTRACT

Thin film based surface acoustic wave (SAW) technology has been extensively explored for physical, chemical and biological sensors. However, these sensors often show inferior performance for a specific sensing in complex environments, as they are affected by multiple influencing parameters and their coupling interferences. To solve these critical issues, we propose a methodology to extract critical information from the scattering parameter and combine machine learning method to achieve multi-parameter decoupling. We used AlScN film-based SAW device as an example, in which highly c-axis orientated and low stress AlScN film was deposited on silicon substrate. The AlScN/Si SAW device showed a Bode quality factor value of 228 and an electro-mechanical coupling coefficient of ~2.3%. Two sensing parameters (i.e., ultraviolet or UV and temperature) were chosen for demonstration and the proposed machine-learning method was used to distinguish their influences. Highly precision UV sensing and temperature sensing were independently achieved without their mutual interferences. This work provides an effective solution for decoupling of multi-parameter influences and achieving anti-interference effects in thin film based SAW sensing.

Surface acoustic wave (SAW) devices have been widely used for sensors such as

mass[1,2],temperature[3,4], humidity[5-7], UV [8-10], gas molecules[11,12] and biomolecules[12,13]. Conventional SAW devices are fabricated on bulk piezoelectric materials (such as $LiNbO_3$ and Quartz) because of their low cost, smooth surface, stable material parameters, and high acoustic-electric conversion efficiency [2,11]. However, these conventional bulk piezoelectric materials have issues such as limited SAW propagation velocities and/or poor capabilities to be integrated into processes for silicon-based integrated circuits (IC). To overcome these limitations, thin film acoustic wave devices based on piezoelectric thin film materials, such as zinc oxide (ZnO) and aluminum nitride (AlN), have been developed, as these piezoelectric films can be deposited onto non-piezoelectric substrates such as silicon with the advantage of IC process compatibility. Compared to ZnO films, AlN films show a much higher SAW velocity [14], which is suitable for high frequency (thus high sensitivity) sensing, and have advantages of better mechanical properties [15], better chemical stability in acid/alkali, and higher operating temperatures [9, 16]. However, AlN films have low electromechanical coupling coefficients (K^2) such as ~0.5%, which is much lower than those of other piezoelectric materials ($LiNbO_3$, 7%) or thin films (ZnO, 2%)[17]. This severely limits its application in sensors. To solve this engineering challenge, researchers have developed AlScN film, in which an appropriate concentration of scandium (Sc) doped in AlN films can significantly improve the piezoelectric properties of AlN. For example, K^2 value of AlScN based SAW devices can be increased up to 4% [18], which is suitable for high performance sensors and integrated lab-on-chips [19].

Although there are rapid developments with thin film-based SAW technology, severe challenges are still remained for their successful applications. For example, one of the key challenges to develop highly sensitive SAW sensors is that it is simultaneously sensitive to multiple parameters or factors (e.g., temperature, UV, humidity, vibration or electromagnetic noise, etc.), apart from the real and targeted parameters. One commonly applied solution is to use a differential circuit to eliminate the interferences of other parameters [15], however, this often leads to complicated signal processing circuit and test equipment. Another commonly used method is to find the

differences based on different wave modes of the same SAW device[20,21]. However, this method has some limitations, for example, it cannot be applied to various types of SAW devices. Therefore, great challenges are still remained to decouple multi-sensitive parameters of thin film-based SAW sensors.

In this study, we proposed to extract multiple features from scattering parameters of SAW device and then use machine learning methods (i.e., using support vector machine (SVM)[22, 23] and random forest regression (RFR) [24-26]) for training models to distinguish multiple sensitive signals and achieve multi-parameter decoupling. In this study, we will take AlScN film SAW device as an example. Highly c-axis orientated and low stressed AlScN (with Sc concentration of ~9%) film was deposited on silicon, and AlScN film-based SAW devices were fabricated (**Figure** 1a&b). Its Bode Q value is up to 228, and its K^2 value is ~2.3%. We selected two sensitive parameters of UV and temperature as demonstration examples (**Figure** 1a&b). The information extracted from the SAW's transmission parameters (e.g., S_{21}) was used as features, and sensitive parameters (e.g., ambient temperature and UV intensity) were set as labels into the model for training, and then the relationship between the features and the labels using the machine learning methods were fit to obtain a trained model which predicted the corresponding sensitive parameters (see **Figure** 1c). Both high-precision UV sensing and temperature sensing were independently achieved without the interferences by each other for these AlScN film-based SAW devices.

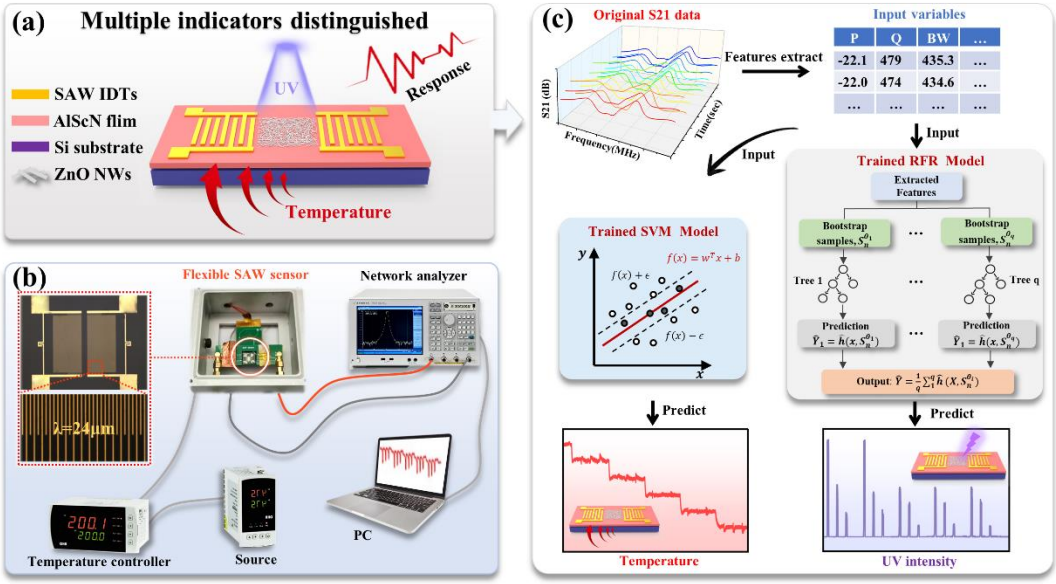

Figure.1 (a) Schematic structure of AlScN film-based SAW devices and schematic sensing diagram of temperature and UV sensing; (b) Schematic view of the testing system used for temperature and UV sensing of AlScN film-based SAW; (c) Model of machine-learning for AlScN film-based SAW sensors.

AlScN films were deposited on silicon using a magnetron sputtering system. Crystal orientation, surface morphology, cross-sectional morphology, element composition and molecular structure of AlScN film were characterized and detailed procedures were shown in supporting information (**SI**). Standard UV photolithography and lift-off processes were used to fabricate two-port SAW resonators on the AlScN/Si layered structure with different wavelengths (λ) of 16, 20, and 24 μm, with their detailed information shown in **SI**. The transmission (S_{21}) and reflection (S_{11}) spectra of the SAW devices were obtained using a vector network analyzer (Ceyear 3656D, China). We selected two SAW sensitive parameters as demonstrators, i.e., UV and temperature. The UV and temperature testing procedures are shown in **SI**. We conducted 16 groups of UV response experiments at 16 different temperature points (from 30 to 50 °C), as listed in **Table S1**.

Figure 2a shows a single and sharp peak at two theta angle of 35.9º in the X-ray diffractometer (XRD) spectrum, indicating that the deposited AlScN film has a preferred (0002) crystal orientation. The full width at half-maximum of the (0002)

crystal orientation for XRD curve is 0.0498°, corresponding to an estimated mean grain size of about 43.39 nm based on the Scherrer's equation[5]. The axial stress was estimated to be ~25.53 MPa, showing that the deposited film has a low residual stress on the Si substrate. Inset in **Figure 2a** shows surface morphology and roughness of the film, and the root-mean square roughness (RMS) was measured to be ~1.17 nm over an area of 10 × 10 μm^2, which is much smoother than that reported in a previous study [27]. **Figure 2b** shows a scanning electron microscope (SEM) image of the AlScN film, revealing the columnar structures of AlScN nanocrystals, perpendicular to the substrate with an average thickness of ~2 μm. Results show that a high-quality AlScN piezoelectric film with c-axis preferred orientation, low stress, and low surface roughness has been deposited on Si substrate.

From the X-ray photoelectron microscope (XPS) analysis, two binding energy components of N 1s were obtained after peak deconvolution using a curve-fitting program, and those at binding energies of 397.25 and 400.20 eV are corresponding to Al-N and Sc-N bonds, as shown in **Figure 2c.** Energy dispersive spectroscopy (EDS) in **Figure 2d** indicate that the Al, Sc, N elements in the AlScN thin films have uniform distributions and the obtained percentages of N, Al and Sc elements are 35.91 wt.%, 55.25 wt.% and 8.84 wt.% respectively, corresponding to 53.33 at%, 42.59 at% and 4.09 at%, respectively.

Figures 2e~g shows electrical performance of AlScN/Si SAW devices, showing clear generations of Rayleigh resonance peaks with resonant frequencies of 309.61, 250.25 and 209.16 MHz for the λ of 16, 20 and 24 μm. We have fabricated four batches of SAW devices and their resonant frequencies with the same wavelength are very close (with relative deviation less than 0.05%). The phase velocities (v_p) of these SAW devices, $v_p = \lambda f_0$, were calculated to be 4953.76, 5005.00 and 5019.84 m.s^{-1}, respectively, which are increased gradually with an increase in wavelength from 16 to 24 μm. High performance SAW devices and high precision SAW sensors should have both the high Q value and K^2. We have obtained the Q value of 228 and K^2 of 2.3% for the device with a λ of 24 μm, showing much better performance than that of AlScN/Si SAW device

reported in Ref. [28].

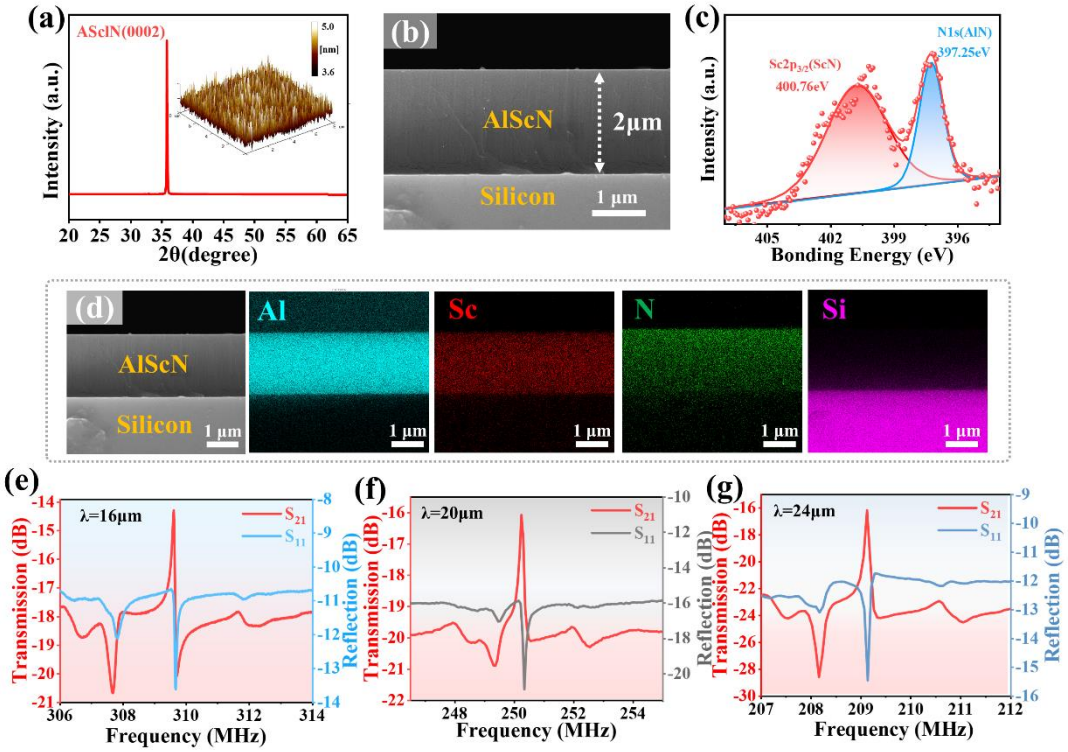

Figure. 2 Characterization of AlScN thin film deposited on the silicon wafer substrate: (a) XRD pattern of the AlScN film, showing strong (0002) orientation; and AFM image of the AlScN film, showing the smooth surface; (b) SEM image of the cross-section of the AlScN film; (c) XPS high-resolution spectra of Al 2p and N 1s of the AlScN films. (d) The element distribution in the AlScN/Si layered structure obtained using an EDS; (e~g) The transmission and reflection spectra of AlScN/Si SAW devices.

Figures 3a and **S1** show the changes of resonant frequency, phase angle and insertion loss of the SAW device (λ of 24 μm) under different UV intensities and various temperatures (testing condions are listed in **Table S1**). When the testing temperature is 30.4 °C, the frequency shifts of the resonance increase with the increase in UV light intensity, as shown in **Figure 3a**. In addition, the phase angles and insertion loss of the resonant mode are observed to increase simultaneously with the increase in UV intensity as shown in **Figures 3a .** As it is well-known, UV responses of SAW devices are mainly based on acoustoelectric effects. The generated free carriers (electron-hole pairs) induced by the UV irradiations interact with the acoustic waves field, resulting

in the changes of transmission characteristics including acoustic wave velocity, attenuation of wave amplitude and phase angle. These changes of the SAW properties can be written using the following equation [29]

$$\frac{\Delta v}{v} = \frac{v - v_{sc}}{v_{oc}} - \frac{k^2}{2} \frac{1}{1+(\sigma_d/\sigma_M)^2} \quad (1)$$

$$\Gamma = \frac{k^2}{2} \frac{\pi}{\lambda} \frac{\sigma/\sigma_M}{1+(\sigma/\sigma_M)^2} \quad (2)$$

$$\Delta\varphi = 2\pi \frac{L}{\lambda} \frac{\Delta v}{v} \quad (3)$$

where v_{oc} is the SAW velocity on a free surface, Δv is the velocity shift, k^2 is the effective electromechanical coupling coefficient, σ is the sheet conductivity, σ_M is a material constant, Γ is the attenuation, λ is the SAW wavelength, $\Delta\varphi$ is the phase angle and L is the acoustic path length.

When the SAW device is at a higher temperature (e.g., 35.2°C), UV responses of the SAW device show similar trends. However, the change of temperature (e.g., from 30.4°C to 35.2°C) will also change the resonant frequency, phase, insertion loss and other characteristics of SAW devices (**Figures 3a**). These resutls demonstrated that both the UV and temperature will affect the characteristics of SAW devices and would interfere with each other.

We selected two sensitive parameters, i.e., UV and temperature, as examples, and apply machine learning algorithms to distinguish these two sensitive parameters. In order to improve the accuracy of machine learning algorithms, we need to maximize the extracted useful information from the original data as features, and then use these features as the inputs of machine learning algorithms. The frequeny responses within the frequency band (205MHz~210MHz, near the resonant frequency) of S_{21} spectra were chosen as the original data. Frequency-amplitude responses of S_{21} in this band were composed of 201 points and regarded as a 201-dimensional vector. Each original vector was assumed to reduce dimension by a nonlinear mapping to obtain 11 features, including Frequency (F), Amplitude (A), Band width (BW), Center frequency (CF), Insertion Loss (IL), Phase (P), Q value (Q), Hausdorff distance (HD), Edit distance on

real sequence (EDR), Maximum value (Max), Dynamic time warping (DTW). These features include the intrinsic physical variation characteristics of the SAW responses (e.g., F, A, BW, CF, IL, P, Q) and the variation characteristics for the S_{21} curves of the SAW device (e.g., HD, EDR, DTW, MAX)[30-32]. Reducing dimension using a nonlinear mapping is beneficial for simplifying calculations and preventing the over-fitting. The calculation methods for these 11 features are shown in the **SI** for more details. These eleven features are changed with the changes of UV intensity from 0.033 mw/cm² to 0.403 mw/cm², at the temperature of 31.7°C as shown in **Figure S2**.

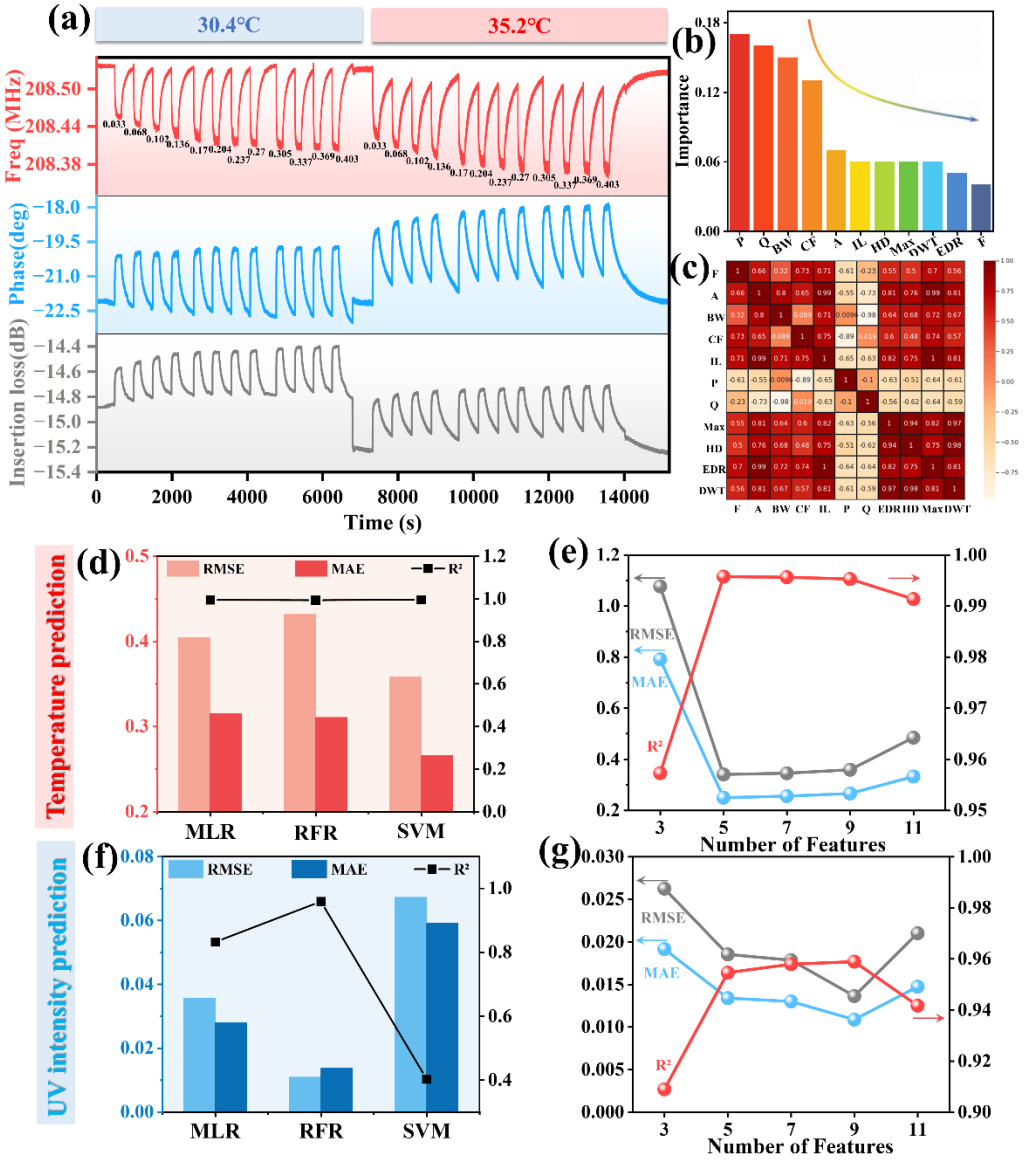

Figure. 3 (a) Frequency, insertion loss, and phase responses of SAW devices under different UV light intensity and temperature; (b) Importance of each feature; (c)Different features Correlation coefficient matrix; (d) The performance of three algorithm (MLR, RFR and SVM) on temperature

prediction; (e) The metrics of MAE, RMSE and R^2 for temperature prediction results using different number of features (3,5,7,9,11); (f)The performance of three algorithm (MLR, RFR and SVM) on UV intensity prediction; (g)The metrics of MAE, RMSE and R^2 for UV light intensity prediction results using different number of features (3,5,7,9,11).

We used three metrics including mean absolute error (MAE), root mean-square error (RMSE) and R^2 values to evaluate the performance of the model [33]. The MAE is defined by Eq. (4).

$$MAE = \frac{1}{n}\Sigma_{i=1}^{n}|y_i - \hat{y}_i| \quad (4)$$

where n represents the number of observations, y_i represents the experimental values, and $\hat{y}_i$ represents the predicted values. This metric calculates the mean of the absolute sum of the errors of the predicted and true values, and is used to evaluate how close the predicted results are to the real data. A smaller MAE value indicates a higher accuracy of the prediction results. Whereas RMSE is frequently used to measure the differences between values predicted by the model and the observed experimental values. The RMSE should be as small as possible, which is defined as

$$RMSE = \sqrt{\frac{\Sigma_{i=1}^{n}(y_i-\hat{y}_i)^2}{n}} \quad (5)$$

R^2 is another indicator that indicates how closely the predicted values from a model matched with the observed values, and is defined as:

$$R^2 = 1 - \frac{\Sigma_{i=1}^{n}(y_i-\hat{y}_i)^2}{\Sigma_{i=1}^{n}(y_i-\bar{y}_i)^2} \quad (6)$$

The ideal R^2 value for a model should be 1. The closer it is to 1, the stronger the model's ability to interpret the predicted value, and the better the model fits the data.

We have compared the performance of three different machine learning regression algorithms, i.e., multiple linear regression (MLR), support vector machine (SVM) and random forest regression (RFR), for the temperature and UV light intensity predictions (**Figures 3d&f**). Results show that the SVM model shows the best performance for temperature prediction, which generates the smallest prediction error (using the MAE

and RMSE) and the largest R^2. The RFR model has the best performance in UV light intensity prediction. Accordingly, we chose to use the SVM model to predict temperature, and use the RFR model to predict UV light intensity. The feature data of the training set were put into these two models with temperature labels and UV intensity labels, respectively, for training processes. The testing sets were then used to evaluate the model's performance. By comparing the actual temperatures and UV light intensities from the experiments with the predicted ones, the prediction accuracy of the model was evaluated.

It is well-known that different features do not contribute equally to model, and some features may be highly correlated with each other, which can result in redundant features[34]. Too many or invalid features will lead to performance degradation of the proposed model. The correlation coefficient matrix (**Figure 3b**) and estimated importance of each feature obtained using a random forest algorithm [33], were used to determine the priority of features (**Figure 3c**). The top 3, 5, 7, 9, and 11 features with the highest importance were selected to construct the model, and their performance on temperature and UV intensity predictions was compared. The results are shown in **Figures 3e&g**. When the number of input features is 5, the model has the best temperature prediction effect with the smallest error (MAE=0.25, RMSE=0.34), and also the largest R^2 of 0.996). For UV light intensity predictions, the optimal number of input features is 9 (with values of MAE=0.011, RMSE=0.0136, and R^2=0.959). Therefore, in the follow-up studies, the SVM model with 5 features was used to predict temperature, and the RFR model with 9 features was used for UV light intensity prediction. Both these two models include 5 features: i.e., Phase, Q value, Band width, Center frequency and Amplitude. Compared with those temperature predictions, UV intensity predictions require extra four features (e.g. Hausdorff distance, Maximum value, Dynamic time warping and Insertion Loss).

After optimizing the model algorithm, we further did UV test using the fabricated SAW devices to verify the proposed model, by varying temperatures from 50°C to 31°C. **Figure 4a** shows that the obtained resonant frequency responses of the SAW device

under dynamically changed temperatures and ultraviolet environments.

In order to show the temperature prediction results of the model, we used the traditional linear regression and our model after training based on SVM to predict the temperature value of the test data, and their results were then compared with the actual values. The obtained results are shown in **Figure 4b**, which indicates that due to the interference of ultraviolet environment, the traditional linear regression (i.e., using a linear function fitting based on the relationship between frequency and temperature) has a larger deviation in temperature prediction. Whereas our newly proposed training model has shown a better prediction effect, proving the validity of our proposed SVM in SAW temperature prediction.

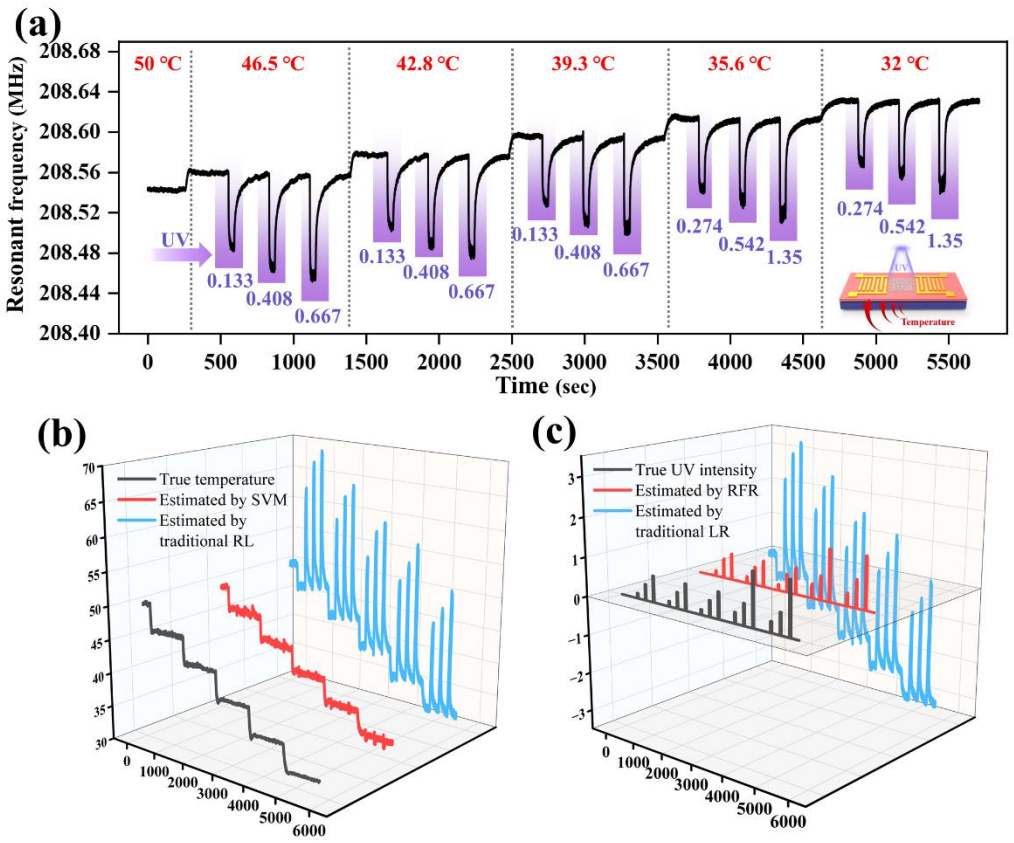

Figure 4 (a) Resonant frequency of SAW devices under different UV light intensity and temperature (Test experiment). (b) Comparison of the temperature predicted results by the traditional linear regression and SVM model (c) Comparison of the UV intensity predicted results by the traditional linear regression and RFR model.

Similarly, the prediction results of UV intensity are shown in **Figure 4c.** When using the traditionally linear regression for UV analysis, the analysis results are deviated significantly from the actual UV intensity data. This is because the frequency changes caused by the temperature changes were also treated as the influences of UV changes. However, when the results of SAW devices were compared to those obtained from our proposed machine learning method (RFR), the predicted results agreed well with the actual UV intensities.

We further did multiple UV sensing tests with temperatures varied from 32°C to 38°C for the SAW devices with wavelengths of 20 μm and 16 μm, and the obtained results are shown in **Figures S3** and **S4**. Results demonstrate that the proposed machine-learning algorithm effectively achieve decoupling of multiple parameters and our model is applicable to the different SAW devices with different wavelengths. All these results clearly demonstrate the potentials using the proposed machine learning method to enable SAW device realizing accurate measurement of multiple physical quantities at the same time.

In brief, highly c-axis orientation and low-stressed AlScN film was deposited on silicon substrate in this study. The AlScN film-based SAW devices showed a Q value up to 228, and K^2 of 2.3%. We then proposed a strategy by extracting more information from the scattering parameter, and combined the machine learning method (e.g., SVM and RFR) to train a model to achieve multi-parameter decoupling for AlScN film-based SAW device. As proof-of-concept demonstrations, we took UV and temperature sensing as examples, and we have demonstrated the effective decoupling of these two parameters, simultaneously and accurately. This work provides an effective solution for multi-parameter decoupling of film-based SAW sensor and realizing high-precision anti-interference sensing.

SUPPLEMENTARY MATERIAL

See supplementary material for the detailed calculation methods about 11 Features of SAW, all experimental data used for model training and model prediction results of

SAW devices based on different wavelengths.

AUTHOR DECLARATIONS

Conflict of Interest

The authors have no conflicts to disclose.

Author Contributions

The manuscript was written through contributions of all authors. All authors have given approval to the final version of the manuscript.

DATA AVAILABILITY

The data that support the findings of this study are available from the corresponding authors upon reasonable request

ACKNOWLEDGMENTS

This work was supported by the NSFC (No.52075162), The Program of New and High-tech Industry of Hunan Province (2020GK2015, 2021GK4014), The Joint Fund Project of the Ministry of Education, The Excellent Youth Fund of Hunan Province (2021JJ20018), the Key Research & Development Program of Guangdong Province (2020B0101040002), International Exchange Grant (IEC/NSFC/201078) through Royal Society UK and the NSFC.

REFERENCES

1. Jiangpo Zheng, Jian Zhou, Pei Zeng, Yi Liu, Yiping Shen, Wenze Yao, Zhe Chen, Jianhui Wu, Shuo Xiong, Yiqin Chen, Xianglong Shi, Jie Liu, Yongqing Fu, and Huigao Duan, Applied Physics Letters 116 (12), 123502 (2020).
2. Zhe Chen, Jian Zhou, Hao Tang, Yi Liu, Yiping Shen, Xiaobo Yin, Jiangpo Zheng, Hongshuai Zhang, Jianhui Wu, Xianglong Shi, Yiqin Chen, Yongqing Fu, and Huigao Duan, ACS Sensors **5** (6), 1657 (2020).
3. Jian Zhou, Dinghong Zhang, Yanghui Liu, Fengling Zhuo, Lirong Qian, Honglang Li, Yong-Qing Fu, and Huigao Duan, Record-breaking frequency of 44 GHz based on the higher order mode of surface acoustic waves with LiNbO3/SiO2/SiC heterostructures Engineering (2022).
4. Leonardo Lamanna, Francesco Rizzi, Francesco Guido, Luciana Algieri, Sergio Marras, Vincenzo Mariano Mastronardi, Antonio Qualtieri, and Massimo De Vittorio, Flexible and Transparent Aluminum-Nitride-Based Surface-Acoustic-Wave Device on Polymeric Polyethylene Naphthalate. Advanced Electronic Materials **5** (6), 1900095 (2019).

5. Jianhui Wu, Changshuai Yin, Jian Zhou, Honglang Li, Yi Liu, Yiping Shen, Sean Garner, Yongqing Fu, and Huigao Duan, Ultrathin Glass-Based Flexible, Transparent, and Ultrasensitive Surface Acoustic Wave Humidity Sensor with ZnO Nanowires and Graphene Quantum Dots. ACS Applied Materials & Interfaces **12** (35), 39817 (2020).
6. Jian Zhou, Zhangbin Ji, Yihao Guo, Yanghui Liu, Fengling Zhuo, Yuanjin Zheng, Yuandong Gu, YongQing Fu, and Huigao Duan, Strategy to minimize bending strain interference for flexible acoustic wave sensing platform npj Flexible Electronics **6** (1), 84 (2022).
7. Jian Zhou; Yanghui Liu; Zhengjia Zhan; Fengling Zhuo; Zhangbin Ji; Yuanjin Zheng; Yongqing Fu; Huigao Duan, Strategies for Giant Mass Sensitivity Using Super-High-Frequency Acoustic Waves. IEEE Sensors Journal, 2022. 22(21): p. 20336-20345.
8. Changshuai Yin, Jianhui Wu, Jian Zhou, Dinghong Zhang, Zhijin Liu, Xudong Liu, Lizhu Liu, Zhengjia Zhan, Sean Garner, and Yongqing Fu, Enhancing the sensitivity of flexible acoustic wave ultraviolet photodetector with graphene-quantum-dots decorated ZnO nanowires. Sensors and Actuators A: Physical **321**, 112590 (2021).
9. Zhangbin Ji, Jian Zhou, Huamao Lin, Jianhui Wu, Dinghong Zhang, Sean Garner, Alex Gu, Shurong Dong, YongQing Fu, and Huigao Duan, Flexible thin-film acoustic wave devices with off-axis bending characteristics for multisensing applications. Microsystems & Nanoengineering **7** (1), 97 (2021).
10. Yihao Guo, Jian Zhou, Zhangbin Ji, Yanghui Liu, Rongtao Cao, Fengling Zhuo, Kaitao Tan, Huigao Duan, Yongqing Fu, A new strategy to minimize humidity influences on acoustic wave ultraviolet sensors using ZnO nanowires wrapped with hydrophobic silica nanoparticles. Microsystems & Nanoengineering, 2022. 8(1): p. 121.
11. Shuo Xiong, Jian Zhou, Jianhui Wu, Honglang Li, Wei Zhao, Chenguang He, Yi Liu, Yiqin Chen, Yongqing Fu, and Huigao Duan, Acoustic Wave Nitrogen Dioxide Sensor with Ultraviolet Activated 3D Porous Architecture of Ag-Decorated Reduced Graphene Oxide and Polypyrrole Aerogel. ACS Applied Materials & Interfaces **13** (35), 42094 (2021).
12. Sijia Liang, Dennis Finck, Marc W. Neis, Jutta Schwarzkopf, Dirk Mayer, and Roger Wördenweber, SAW gas sensor based on extremely thin strain-engineered K0.7Na0.3NbO3 films. Applied Physics Letters **119** (11), 112905 (2021).
13. Junwang Ji, Yiquan Pang, Dongxiao Li, Zheng Huang, Zuwei Zhang, Ning Xue, Yi Xu, and Xiaojing Mu, An aptamer-based shear horizontal surface acoustic wave biosensor with a CVD-grown single-layered graphene film for high-sensitivity detection of a label-free endotoxin. Microsystems & Nanoengineering **6** (1), 4 (2020).
14. Y. Q. Fu, J. K. Luo, N. T. Nguyen, A. J. Walton, A. J. Flewitt, X. T. Zu, Y. Li, G. McHale, A. Matthews, E. Iborra, H. Du, and W. I. Milne, Advances in piezoelectric

thin films for acoustic biosensors, acoustofluidics and lab-on-chip applications. Progress in Materials Science **89**, 31 (2017).

15. Fanbing Hu, Lina Cheng, Shuyao Fan, Xufeng Xue, Yong Liang, Minghui Lu, and Wen Wang, Chip-level orthometric surface acoustic wave device with AlN/metal/Si multilayer structure for sensing strain at high temperature. Sensors and Actuators A: Physical **333**, 113298 (2022).
16. Shuo Xiong, Xudong Liu, Jian Zhou, Yi Liu, Yiping Shen, Xiaobo Yin, Jianhui Wu, Ran Tao, Yong Qing Fu, and Huigao Duan, Stability studies of ZnO and AlN thin film acoustic wave devices in acid and alkali harsh environments. Rsc Advances **10** (33), 19178 (2020).
17. Jian Zhou, Xingli He, Hao Jin, Wenbo Wang, Bin Feng, Shurong Dong, Demiao Wang, Guangyi Zou, and J. K. Luo, Crystalline structure effect on the performance of flexible ZnO/polyimide surface acoustic wave devices. J. Appl. Phys. 2013. 114(4).
18. Wenbo Wang, Patrick M. Mayrhofer, Xingli He, Manuel Gillinger, Zhi Ye, Xiaozhi Wang, Achim Bittner, Ulrich Schmid, and J. K. Luo, High performance AlScN thin film based surface acoustic wave devices with large electromechanical coupling coefficient. Appl. Phys. Lett, **105**(13) 2014.
19. W B Wang, Y Q Fu, J J Chen, W P Xuan, J K Chen, X Z Wang, P Mayrhofer, P F Duan, A Bittner, U Schmid, AlScN thin film based surface acoustic wave devices with enhanced microfluidic performance. J Micromech Microeng, 2016. 26(7).
20. WeiPengXuanJinKaiChenaXingLiHeaWenBoWangaShurongDongaJikuiLuo, Flexible Surface Acoustic Wave Humidity Sensor with on Chip Temperature Compensation. Procedia Engineering, 2015. 120: p. 364-367.
21. Hongsheng Xu, Zhen Cao, Shurong Dong, Jinkai Chen, Weipeng Xuan, Weiwei Cheng, Shuyi Huang, Lin Shi, Shuting Liu, Umar Farooq, Akeel Qadir and Jikui Luo, Flexible dual-mode surface acoustic wave strain sensor based on crystalline LiNbO3 thin film. Journal of Micromechanics and Microengineering, 2019. 29(2).
22. Smola, A.J. and B. Scholkopf, A tutorial on support vector regression. Stat Comput, **14**(3) p 199-222 2004.
23. Hearst, M.A., S.T. Dumais, E. Osuna, J. Platt, B. Scholkopf., Support vector machines. IEEE Intelligent Systems and their Applications, **13**(4) 18-28 1998.
24. Breiman, L., Random Forests. Machine Learning, **45**(1) 2001.
25. Biau, G. and E. Scornet, A random forest guided tour. Test, 2016. 25(2): p. 197-227.
26. Liaw, A. and M.C. Wiener. Classification and Regression by randomForest. 2007.
27. Yuan Lu,Markus Reusch,Nicolas Kurz,Anli Ding,Tim Christoph,Lutz Kirste,Vadim Lebedev,Agnė Žukauskaitė, Surface Morphology and Microstructure of Pulsed DC Magnetron Sputtered Piezoelectric AlN and AlScN Thin Films. Phys. Status Solidi, **215**(9) 2018.
28. Mingyo Park, Zhijian Hao,Rytis Dargis,Andrew Clark,Azadeh Ansari, Epitaxial

Aluminum Scandium Nitride Super High Frequency Acoustic Resonators. J Microelectromech Syst, **29**(4) 490-498 2020.

29. Yi Zhang, Yao Cai, Jie Zhou, Ying Xie, Qinwen Xu, Yang Zou, Shishang Guo, Hongxing Xu, Chengliang Sun, Sheng Liu, Surface acoustic wave-based ultraviolet photodetectors: a review. Sci. Bull, **65**(7) 587-600 2020.
30. Chen, L., M.T. Özsu, and V. Oria, Robust and fast similarity search for moving object trajectories, in Proceedings of the 2005 ACM SIGMOD international conference on Management of data. 2005, Association for Computing Machinery: Baltimore, Maryland. 491–502 2005.
31. Berndt, D.J. and J. Clifford, Using dynamic time warping to find patterns in time series, in Proceedings of the 3rd International Conference on Knowledge Discovery and Data Mining. 1994, AAAI Press: Seattle, WA. 359–370.
32. Huttenlocher, D.P., G.A. Klanderman, and W.J. Rucklidge, Comparing images using the Hausdorff distance. IEEE Transactions on Pattern Analysis and Machine Intelligence, **15**(9) 850-863 1993.
33. Botchkarev, A., A New Typology Design of Performance Metrics to Measure Errors in Machine Learning Regression Algorithms. Interdisciplinary Journal of Information, Knowledge, and Management, 14 045-076 2019.
34. Qian Zhang, Yong Wang , Tao Wang , Dongsheng Li, Jin Xie , Hamdi Torun , Yongqing Fu, Piezoelectric Smart Patch Operated with Machine-Learning Algorithms for Effective Detection and Elimination of Condensation. ACS Sens, **6**(8) 3072-3081 2021.